Ellis Shelby (Orcid ID: 0000-0003-1372-4967)
Partin Judson, Wiley (Orcid ID: 0000-0003-0315-5545)

Extended cave drip water time series captures the 2015 – 2016 El Niño in Northern Borneo

Shelby A. Ellis*[1], Kim M. Cobb[1], Jessica W. Moerman[2], Judson W. Partin[3], A. Landry Bennett[1], Jenny Malang[4], Hein Gerstner[4], Andrew A. Tuen[5]

[1]School of Earth and Atmospheric Sciences, Georgia Institute of Technology, Atlanta, Georgia USA, [2]Human Origins Program, National Museum of Natural History, Smithsonian Institution, Washington, DC USA, [3]Institute for Geophysics, Jackson School of Geosciences, University of Texas at Austin, Austin, Texas USA, [4]Gunung Mulu National Park, Sarawak, Malaysia, [5]Institute of Biodiversity and Environmental Conservation, Universiti Malaysia Sarawak, Sarawak, Malaysia

*Corresponding author: Shelby Ellis, sellis39@gatech.edu

Key Points:

- **Three 12-year-long cave drip water $\delta^{18}O$ time series capture El Niño and La Niña events in Northern Borneo**
- **Estimates of karst residence times range from 3 to 18 months, with a secondary contribution from a longer-term reservoir at one drip site**
- **Drip water non-stationarity implies multiple stalagmites are required to reconstruct El Niño Southern Oscillation variability over time**

This is the author manuscript accepted for publication and has undergone full peer review but has not been through the copyediting, typesetting, pagination and proofreading process, which may lead to differences between this version and the Version of Record. Please cite this article as doi: 10.1029/2019GL086363

Abstract

Time series of cave drip water oxygen isotopes ($\delta^{18}O$) provide site-specific assessments of the contributions of climate and karst processes to stalagmite $\delta^{18}O$ records employed for hydroclimate reconstructions. We present ~12 year-long time series of biweekly cave drip water $\delta^{18}O$ variations from three sites as well as a daily-resolved local rainfall $\delta^{18}O$ record from Gunung Mulu National Park in Northern Borneo. Drip water $\delta^{18}O$ variations closely match rainfall $\delta^{18}O$ variations averaged over the preceding 3-18 months. We observe coherent interannual drip water $\delta^{18}O$ variability of ~3 to 5‰ related to the El Niño-Southern Oscillation (ENSO), with sustained positive rainfall and drip water $\delta^{18}O$ anomalies observed during the 2015/2016 El Niño. Evidence of non-linear behavior at one of three drip water monitoring sites implies a time-varying contribution from a longer-term reservoir. Our results suggest that well-replicated, high-resolution stalagmite $\delta^{18}O$ reconstructions from Mulu could characterize past ENSO-related variability in regional hydroclimate.

Plain Language Summary

Cave stalagmites allow for the reconstruction of past regional rainfall variability over the last hundreds of thousands of years with robust age control. Such reconstructions rely on the fact that differences in the isotopic composition of rainwater set by regional rainfall patterns is preserved as the rainwater travels through cave bedrock to feed the cave drip waters forming stalagmites. Long-term monitoring of rainwater and cave drip water isotopes ground truth the climate to stalagmite relationship across modern-day changes in regional rainfall. Twelve years of monitoring data presented in this study identify individual El Niño-Southern Oscillation (ENSO) events in rainfall and cave drip water isotopic composition, providing a strong foundation for stalagmite-based climate reconstructions from this site.

1. Introduction

Stalagmite oxygen isotope reconstructions provide key insights into past terrestrial hydroclimate variability globally on seasonal to orbital timescales. In some tropical and subtropical regions where rainfall is dominated by strong vertical convection and infrequent year-round temperature variability, the ‘amount effect’ framework aids interpretations of stalagmite oxygen isotope records. Modern empirical observations classify the ‘amount effect’ as a correlation between high (low) rainfall rates on monthly and longer time scales with depleted (enriched) rainfall $\delta^{18}O$ (hereinafter $\delta^{18}O_R$) (Craig, 1961; Dansgaard, 1964; Rozanski et al.,

1992). Using the amount effect framework, overlapping $\delta^{18}O_{stal}$ records from monsoon-vulnerable regions in South America (Cheng et al., 2013; Cruz et al., 2005), Australia (Griffiths et al., 2009), Oman (Burns et al., 1998), and India (Sinha et al., 2005) demonstrate interhemispheric anti-phasing in $\delta^{18}O_R$ variability from precession-driven (~19 – 23ky) orbital forcing. North Atlantic millennial-length Dansgaard-Oeschger (Dansgaard et al., 1993) and Heinrich events (Heinrich, 1988) are mirrored in stalagmite $\delta^{18}O$ records utilizing the amount effect framework from far-off tropical-subtropical locations such as central South America (Wang et al., 2006), China (Wang et al., 2001), and Northern (N.) Borneo (Partin et al., 2007), suggesting a link between high-latitude temperature variations and changes in monsoons (Cheng et al., 2012). Other reproducible stalagmite $\delta^{18}O$ records from N. Borneo (Carolin et al., 2013; 2016; Meckler et al., 2012; Partin et al., 2007) suggest forced changes in Walker circulation properties in the west Pacific warm pool (WPWP), a major source of heat and water vapor for the interannual climate phenomenon the El Niño-Southern Oscillation (ENSO) (Rasmusson and Wallace, 1983). However, to tease apart external and internal climate forcings over high-frequency natural climate phenomenon, such as ENSO, requires sub-annually resolved $\delta^{18}O_{stal}$ records.

Over the last twenty years, the combination of improved high-resolution sampling techniques together with increased temporal resolution, precision, and accuracy of stalagmite U/Th dates have allowed for the generation of absolutely-dated sub-annual to annually resolved stalagmite $\delta^{18}O$ records in stalagmites with relatively fast growth rates. Successful efforts from

high-resolution stalagmite $\delta^{18}O$ records spanning the late Holocene have identified individual tropical cyclones in Belize (Frappier et al., 2007) and Australia (Nott et al., 2007), intraseasonal variation of monsoonal rainfall in Thailand (Cai et al., 2010), annual-length droughts in the Yucatan Peninsula (Medina-Elizalde et al., 2010), and the 1997/1998 El Niño event from a Chinese stalagmite (Liu et al., 2018). In regions where monsoon strength is linked to El Niño-Southern Oscillation (ENSO) extremes, high-resolution stalagmite $\delta^{18}O$ records characterize past precipitation-related anomalies in SE China (Zhang et al., 2018) and N. Thailand (Muangsong et al., 2014), as well as in Panama (Lachniet et al., 2004), Belize (Akers et al., 2016), and Mexico (Lachniet et al., 2012). In Borneo, where ENSO exerts a dominant influence on $\delta^{18}O_R$ (Moerman et al., 2013), a sub-annually-resolved stalagmite $\delta^{18}O$ record resolves a reduction in interannual variability during the mid-Holocene (Chen et al., 2016). Despite the drive towards sub-annually- to annually-resolved stalagmite $\delta^{18}O$ records, the links between large-scale climate, local rainfall $\delta^{18}O$, and cave drip water $\delta^{18}O$ remain poorly constrained.

Long-term rainfall and cave drip water monitoring is critical to the identification of large-scale versus local influences on cave drip water $\delta^{18}O$ variability, and by extension, stalagmite $\delta^{18}O$ variability, through time. Such data form an integral constraint on proxy system models for stalagmite $\delta^{18}O$ (Dee et al., 2015; Partin et al., 2013b), which allow for the transformation of physical climate variables to stalagmite $\delta^{18}O$ variability. For $\delta^{18}O_R$ variability, the amount effect remains an interpretative framework for tropical stalagmite $\delta^{18}O$ records (Lachniet et al., 2004; 2009), although many studies document a range of additional local-scale controls on modern

rainfall $\delta^{18}O_R$. In the tropics, influencing hydroclimate processes over $\delta^{18}O_R$ composition include upstream rainout (Konecky et al., 2019), moisture source convergence (Cai and Tian, 2016), and precipitating cloud type (Aggarwal et al., 2016). Once the rainwater falls to the ground, evaporative enrichment may alter the $\delta^{18}O_R$ signal as it infiltrates into the karst zone (Cuthbert et al., 2014). Because stalagmite $\delta^{18}O$ reconstructions reflect amount-weighted drip water $\delta^{18}O$ variations, it is important to quantify the high frequency (daily to intraseasonal) as well as lower frequency (interannual to sub-decadal) controls on rainfall and cave drip water $\delta^{18}O$ variability at a stalagmite $\delta^{18}O$ reconstruction site. Additional factors that govern the rainfall-to-drip water transformation include the size of the vadose zone (Ford and Williams, 2007), the degree of interaction between different reservoirs across the vadose zone (Fairchild et al., 2006), and the preferred recharge flow pathway (Fairchild and Baker, 2012). Karst water routing can vary appreciably through time, with a wide range of water transit times implied by cave drip water $\delta^{18}O$ (hereinafter $\delta^{18}O_{dw}$) variability within the same cavern (Partin et al., 2013a; Treble et al., 2013; Zhang and Li, 2019). Indeed, long-term monitoring of rainfall and cave drip waters remain crucial to quantify the robustness of stalagmite $\delta^{18}O$-based climate reconstructions at individual paleoclimate sites.

In this paper we present a daily rainfall $\delta^{18}O$ time series (2006 – 2018) paired with the longest biweekly cave drip water $\delta^{18}O$ time series (2007 – 2018) from Gunung Mulu National Park, home to numerous stalagmite $\delta^{18}O$-based reconstructions (Partin et al., 2007; Carolin et al., 2013, 2016; Meckler et al., 2012; Chen et al., 2016). This study builds on similar work presented

by Moerman et al. (2013, 2014), in that it extends Mulu $\delta^{18}O_R$ and $\delta^{18}O_{dw}$ time series through the very strong 2015/16 El Niño event. Using the $\delta^{18}O_R$ as input to simulate the observed $\delta^{18}O_{dw}$ variations at three sites, we constrain the residence times of karst waters and assess the linearity of the $\delta^{18}O_R$ to $\delta^{18}O_{dw}$ transformation at this key site.

2. Methods

This study extends one rainfall and three cave drip water time series first presented by Moerman et al. (2014) from Gunung Mulu National Park in N. Borneo (4°06'N, 114°53'E) (Figure S1). For a detailed description of the geologic and climatic setting of Gunung Mulu, the reader is referred to previous studies (Cobb et al., 2007; Moerman et al., 2013; Partin et al., 2013a; Carolin et al., 2016). Rainfall samples were collected by Mulu Airport Meteorological staff using a splayed-bottom, copper rain gauge (Casella model M1144003), following the sampling protocol outlined in Moerman et al. (2013). Rainfall and cave drip water samples were collected and stored in 3 mL glass vials and sealed with rubber stoppers and aluminum crimp-tops to reduce evaporation prior to analysis. All samples were measured for $\delta^{18}O$ and δD using a Picarro L2130-i cavity ring-down water isotope analyzer, with a long-term precision better than ± 0.1‰ and ± 0.5‰ (1σ, N > 500), respectively, following analytical procedures outlined in Moerman et al., 2013.

Cave drip water samples reflect two distinct sampling strategies: (1) quasi bi-weekly collection at three established drip sampling sites by park staff (Figure S2) and (2) collections spanning most of the Gunung Mulu formation conducted during large field expeditions (Figure

S1). For each drip water collection, corresponding drip rates were recorded in drips per minute (dpm). The Wind Fast (WF) and Wind Slow (WS) drip sites are located ~75m from the entrance to Wind Cave, roughly ~20m apart dripping at 32 ± 7 dpm (1σ) and 7 ± 1 dpm (1σ). The L2 drip site is located ~140m from the entranced to Lang's Cave, which is approximately 5km south of Wind Cave, and drips at 15 ± 3 dpm (1σ). All three drip water time series contain two significant sampling hiatuses: Feb-July, 2014 and Sep, 2014-Aug, 2015. Spatial surveys of both stalagmite-forming and non-stalagmite-forming drip waters were collected during field expeditions in Aug, 2008 (N = 63), Feb/Mar, 2010 (N = 128), Oct/Nov 2012 (N = 291), Feb/Mar 2013 (N = 37), May, 2016 (N = 92), May, 2017 (N = 180), and Mar/Apr, 2018 (N = 124) (Figures S3, S4, S5).

Two proxy system models (PSMs) were used to model the transformation of $\delta^{18}O_R$ to $\delta^{18}O_D$, generating estimates of karst residence times (τ) given one or two drip water reservoirs at Mulu following Moerman et al. (2014). The autogenic recharge model (hereafter ARM) generates an ensemble of modelled drip water time series' through a backwards projected running mean of averaged daily amount-weighted local $\delta^{18}O_R$ for different averaging intervals, or residence times. The bivariate mixing model (hereafter BMM) assigns $\delta^{18}O$ values for two reservoirs (A and B) that mix to form cave $\delta^{18}O_{dw}$. The equation for BMM is as follows:

$$\mathbf{X_M = X_A(1 - f_B) + X_B f_B}$$

where X_A and X_B are the isotopic composition of reservoir A and B, respectively and f_A and f_B are the reservoir A and B mixing ratios, respectively. Throughout the manuscript, the significance of observed Pearson's correlation coefficients is assessed using a student's t-test,

where the degrees of freedom have been modified to reflect serial autocorrelation in the data following Bretherton et al. (1999).

3 Results

3.1 Rainfall $\delta^{18}O$ variability across ENSO extremes

Daily $\delta^{18}O_R$ values vary appreciably across the 12-yr time series, ranging from -1.6 to -24.3‰ (Figure 1b) with an average of -7.3 ± 3.7‰ (1σ, N = 2,664), and δD ranges from -85.4 to -153.8‰ with an average of -45.6 ± 29.6‰ (1σ, not pictured). Daily rainfall amounts range from 0 to 300.3 mm/day (Figure 1e) averaging 13.8 ± 22.4 mm/day. Seasonal variability is absent in both rainfall amount and in $\delta^{18}O_R$, consistent with previous studies in N. Borneo (Moerman et al., 2013; Kurita et al., 2018).

Significant correlations between rainfall amount and rainfall $\delta^{18}O$ exist on weekly to interannual timescales at Gunung Mulu. Daily Mulu $\delta^{18}O_R$ values are significantly correlated to local rainfall averaged over the previous 5-8 days ($R=-0.39$, $p<0.05$), and to Outgoing Longwave Radiation (OLR) averaged over the preceding 5-8 days ($R=-0.45$, $p<0.05$; Figure S6a). Our results suggest a water vapor residence time of roughly one week, in line with previous estimates from the site (Moerman et al., 2013). We observe the strongest relationship between Mulu $\delta^{18}O_R$ and Mulu rainfall when both variables are averaged over monthly or longer timescales (Figures S6b, Table S1). For annually-averaged data, the correlation between rainfall amount and rainfall $\delta^{18}O$ reaches -0.67 ($p<0.05$).

ENSO is the dominant driver of rainfall $\delta^{18}O$ variability in N. Borneo, whereby El Niño and La Niña events drive decreases and increases in regional precipitation, respectively, that influence daily to interannual $\delta^{18}O_R$ variability. Over the entire dataset, $\delta^{18}O_R$ is significantly correlated to ENSO indices such as the NIÑO4 index of western equatorial Pacific sea surface temperature (SST) anomalies ($R(\delta^{18}O_R$, NIÑO4 SST)=0.64, $p<0.05$; Figures 1a and 1b, Table S2). Local rainfall amount exhibits weaker but still significant correlations to ENSO indices (e.g. $R(\delta^{18}O_R$, NIÑO4= -0.38); $p<0.01$) (Table S2). The 2009/10 and 2015/16 El Niño events caused ~50 and 90 days of significantly enriched daily $\delta^{18}O_R$ values up +1.0‰ in January-February-March (JFM) (with respect to mean JFM values (-6.1 ± 2.2‰; Figure S7)). Conversely, the 2007/08 and 2010/11 La Niña events were associated with significant decreases in daily $\delta^{18}O_R$ of up to -18.5‰ during JFM, albeit with a larger isotopic spread (Figure S7).

3.2 Cave drip water $\delta^{18}O$ variability as a function of local rainfall $\delta^{18}O$

Drip water $\delta^{18}O$ values for Wind Fast and Wind Slow $\delta^{18}O_{dw}$ range from -3.7 to –11.6‰ and -3.4 to -11.7‰, respectively, while values for Lang's Cave range from –5.9 to –10.0‰ (Figure 1c). Wind Fast (WF) and Wind Slow (WS) $\delta^{18}O_{dw}$ values average -7.9 ± 1.3‰ (1σ, N = 253) and -7.7 ± 1.3‰ (1σ, N = 254), respectively, and Lang's Cave (L2) $\delta^{18}O_{dw}$ average -8.1 ± 0.7‰ (1σ, N = 253), statistically indistinguishable from the amount-weighted average of Mulu $\delta^{18}O_R$ (-8.4 ± 2.4‰, Figure 1c). Mulu amount-weighted $\delta^{18}O_R$ overlaps all three cave $\delta^{18}O_{dw}$ time series mean values, an unique trait not observed at other tropical cave $\delta^{18}O_{dw}$ sites whose

amount-weighted precipitation is generally more positive than cave $\delta^{18}O_{dw}$ (Baker et al., 2019). There is no clear relationship between $\delta^{18}O_{dw}$ and drip rate, nor local rainfall and drip rate, on any timescale (Figure 1d).

All three cave $\delta^{18}O_{dw}$ time series display coherent interannual fluctuations driven by ENSO variability, consistent with our analysis of $\delta^{18}O_R$ variability at the site. WF and WS drips reflect a higher range of interannual $\delta^{18}O_{dw}$ variability (~3 to 5‰) in comparison to L2 (~1 to 2.5‰). All three $\delta^{18}O_{dw}$ time series become more enriched (depleted) during El Niño (La Niña), with anomalies that persist for months following the peak of each event (Figure 1a and 1c). Indeed, $\delta^{18}O_{dw}$ anomalies across all three caves scale with the size of ENSO-related SST anomalies, with the largest excursions observed during the 2015/2016 El Niño event (Figure S8). We observe a strong linear relationship between cave $\delta^{18}O_{dw}$ and NIÑO 3.4 SST anomalies at both Wind cave sites (R^2=0.94 and R^2=0.92 for WF and WS, respectively), whereby El Niño (La Niña) events correspond to enriched (depleted) cave $\delta^{18}O_{dw}$ values (Figure S8). Lang's cave $\delta^{18}O_{dw}$ values are also significantly correlated to NIÑO 3.4 SST values (R^2=0.54, $p<0.05$), but are overall lower than the correlations observed for Wind Cave (Figure S8).

Seven spatial surveys of stalagmite and non-stalagmite forming cave $\delta^{18}O_{dw}$ from nine cave systems reflected system-wide shifts in $\delta^{18}O_{dw}$ associated with ENSO variability. During the largest events (2010 and 2015/2016 El Niño), cave-wide $\delta^{18}O_{dw}$ values exhibited the most spread, as drips with a faster residence time reflected large $\delta^{18}O_R$ anomalies during these times, while some reflected little if any shift from long-term average $\delta^{18}O_{dw}$, possibly indicative of

multi-year residence times (Figure S5). We observed no significant difference in $\delta^{18}O_{dw}$ mean values for stalagmite-forming versus non-stalagmite-forming drips (-7.8 ± 0.8‰ (1σ, N = 356) and -7.5 ± 1.1‰ (1σ, N = 577), respectively (Figure S4).

3.3 Estimates of Mulu karst residence times

Modelled drip water $\delta^{18}O$ time series derived from local rainfall $\delta^{18}O$ allow for the quantification of karst residence times for the three drip water sites, and reproduce up to 85% of the observed drip water $\delta^{18}O$ variability. Karst residence times are estimated using an autogenic recharge model (ARM), where the daily amount-weighted $\delta^{18}O_R$ values are back-averaged over different time intervals (reflecting different karst residence times) to generate a suite of modelled $\delta^{18}O_{dw}$ time series. A best fit between modelled and observed $\delta^{18}O_{dw}$ variability is identified as a maximum in Pearson correlation coefficients and a minimum in the sum of residuals calculated between the modelled and observed $\delta^{18}O_{dw}$ time series. It is important to note that the best fit estimates of residence times are only approximate, as residence times within +/-10% of the best fit yield similarly high correlations between observed and modelled $\delta^{18}O_{dw}$ time series (Table S3). For drips WF and WS, the best fit is obtained for a residence time of 4.5 months (R_{WF}=0.89 and R_{WS} = 0.93, respectively, $p<0.05$; Figure 2a, 2b, and 2c), while the best fit for drip L2 is achieved with a residence time of 10.5 months (R_{L2}=0.85, $p<0.05$; Figure 2d; Table S3). For drip L2, the modelled drip water $\delta^{18}O$ time series overshoots the observed $\delta^{18}O_{dw}$ variations by ~ +1‰ during El Niño events and by ~ -1‰ during La Niña events.

A bivariate mixing model (BMM) that employs two reservoirs - a fast-responding and a slow-responding reservoir - provides a better fit to the L2 $\delta^{18}O_{dw}$ observations relative to the single reservoir model employed in the autogenic recharge model (ARM) used above. For the BMM, we define a short-term Reservoir A that reflects back-averaged rainfall as utilized in the ARM, that mixes with a longer-term Reservoir B that we assign a value of -8.4‰, reflecting the amount-weighted mean $\delta^{18}O_R$ at Mulu over our entire time series. In this model, we simulate the mixing of newly recharged waters (Reservoir A) with older karst waters (Reservoir B). In using the entire 12-yr-long time series to estimate a long-term average value for amount-weighted $\delta^{18}O_R$ at Mulu, we make the assumption that the longer the time series utilized for this purpose, the more accurately the estimate reflects the true long-term average of karst waters at Lang's Cave. That said, the long-term average of Mulu amount-weighted $\delta^{18}O_R$ is poorly constrained, and can only be approximated by the 12-yr average calculated from our time series. We employ two mixing ratios to simulate the observed Lang's Cave L2 $\delta^{18}O_{dw}$ time series: (1) 40% contributions from Reservoir A and 60% from Reservoir B (hereafter referred to as "40:60") and (2) 80% contributions from Reservoir A and 20% from Reservoir B (hereafter referred to as "80:20"), following Moerman et al., 2014. The 40:60 mixing scenario yields a significantly better fit to the observed L2 time series than the single-reservoir ARM model (Table S3; $R=0.86$, $p<0.05$), particularly during the 2009/2010 El Niño event, and during an ENSO-neutral period from 2012 – 2014 (Figure 2e, purple line). The 80:20 mixing scenario also improves on the ARM (Table S3; $R = 0.86$, $p<0.05$), particularly the strongly enriched (depleted) isotopic

excursions associated with large El Niño (La Niña) anomalies (Figure 2e, pink and maroon lines).

Analyses of modelled versus observed drip water $\delta^{18}O$ variations for the Lang's Cave drip uncover evidence for a potential change in the karst water residence time across the 12-yr drip water $\delta^{18}O$ time series. We find an optimal fit between modelled and observed $\delta^{18}O_{dw}$ values for L2 when the residence time for Reservoir A changes from 10.5 months during 2007 – 2014 to 16.75 months during the period 2015 – 2018 (Figure 2e, Table S3). The most enriched $\delta^{18}O_{dw}$ values at L2 occur during the very strong 2015/2016 El Niño, however, this period is marked by a prolonged hiatus in the three cave drip water time series (September 2014 – August 2015) that precludes an investigation of recharge effects during the early phase of the 2015/16 El Niño event. However, we note that the distribution of rainfall intensity during relatively wet (with depleted $\delta^{18}O_{dw}$) versus dry (with enriched $\delta^{18}O_{dw}$) periods is similar (Figure S9), implying that recharge rates are not the primary driver of the inferred change in mixing scenarios (from 40:60 to 80:20) and residence times (10.5 months to 16.75 months) across the Lang's Cave time series.

4. Discussion

Interannual variations from ENSO-driven rainfall $\delta^{18}O$ are evident in all three Mulu cave drip water $\delta^{18}O$ time series, reflecting rainfall $\delta^{18}O$ variations with karst residence times between ~3 to 18 months. Indeed, all three cave $\delta^{18}O_{dw}$ time series are consistent with a relatively simple transformation of $\delta^{18}O_R$ to cave $\delta^{18}O_{dw}$, supporting previous descriptions of diffuse-seepage flow

at Mulu (Cobb et al., 2007; Moerman et al., 2014; Partin et al., 2013a). The shorter karst residence times at Wind cave (4-5 months) implies less homogenization of $\delta^{18}O_R$ and/or less vadose zone mixing with other reservoirs of karst waters, resulting in higher amplitude $\delta^{18}O_{dw}$ variability (-3.7 to -11.7‰). This is especially evident during individual ENSO extremes. The longer karst residence times documented at Lang's Cave (10-17 months) result in smaller $\delta^{18}O_{dw}$ variations (-5.9 to -10.0‰). The residence time differences between Wind and Lang's Caves are somewhat proportional to the karst overburden, whereby larger overburden at Lang's Cave relative to Wind Cave (~200 versus 100m) correlates with longer residence times. It is difficult to compare our residence time estimates with other tropical or ENSO-influenced cave $\delta^{18}O_{dw}$ sites given that (i) most tropical cave $\delta^{18}O_{dw}$ monitoring sites are characterized by high rainfall seasonality and seasonal recharge (Beal et al., 2019; Fleitmann et al., 2004; Jones et al., 2000; Kennett et al., 2012; Lases-Hernandez et al., 2019; Mickler et al., 2004; Partin et al., 2012) and (ii) there are no other multi-year tropical cave $\delta^{18}O_{dw}$ time series that capture ENSO extremes in $\delta^{18}O_{dw}$ (Chen and Li, 2018; Sun et al., 2018; Zhang and Li, 2019). In tropical caves, high rainfall seasonality combined with short karst residence times generate a seasonal bias in cave $\delta^{18}O_{dw}$ variability skewed towards the $\delta^{18}O_R$ of the dominant recharge period (Jones et al., 2000; Lases-Hernandez et al., 2019; Partin et al., 2012). Indeed, Baker et al., (2019) documents this behavior across many tropical karst sites with mean annual temperatures > 16ºC. However, given that Mulu is not characterized by significant differences in seasonal rainfall with no seasonal bias

evident in our cave $\delta^{18}O_{dw}$ time series, we conclude that our observations represent a departure from the patterns presented in Baker et al., (2019).

We provide evidence that cave $\delta^{18}O_{dw}$ values represent a linear transformation of $\delta^{18}O_R$ values, with some evidence for variable input from a longer-term reservoir at select drip water sites. Non-stationary behavior in the Lang's cave drip water $\delta^{18}O$ time series reflects variable karst residence times and/or changes in mixing ratios between a fast-responding and long-term reservoir. Non-stationary behavior in the L2 cave $\delta^{18}O_{dw}$ time series was previously observed by Moerman et al., (2014), potentially from a hydrological extreme. Hydrological extremes impact the hydraulic pressure of karst waters, potentially causing a change in drainage routes and/or aquifer storage (Ford and Williams, 2007). This type of non-stationary behavior is well-documented across a variety of latitudes and climates, including rapid infiltrations of tropical cyclone related rainfall (Lases-Hernandez et al., 2019), changes to drip-rate in SE Australia from rapid infiltration events (McDonald et al., 2007), and in N. England associated with rapid snowmelt events (Baker and Brundsdon, 2003). In the case of the 2015/16 El Niño event, four consecutive seasons of enriched $\delta^{18}O_R$ ($\leq$ -5.0‰) from July 2015 to April 2016 period may have contributed to protracted enriched $\delta^{18}O_{dw}$ values for drip L2's. Alternatively, a significant increase in karst water residence times, perhaps linked to relatively dry conditions during this time, may explain the extended L2 $\delta^{18}O_{dw}$ enrichment.

The fact that ENSO-related changes in Mulu rainfall $\delta^{18}O$ are recorded in Mulu cave drip water $\delta^{18}O$ time series has important implications for the reconstruction of ENSO in Mulu cave

stalagmite $\delta^{18}O$ records. While ENSO anomalies can be resolved in drips fed by sources with residence times as long as ~18 months (Chen et al., 2016), our results demonstrate that the amplitude of ENSO-related cave $\delta^{18}O_{dw}$ variations is inversely correlated to karst water residence times. Indeed, larger spatial surveys of Mulu cave $\delta^{18}O_{dw}$ values during ENSO extremes demonstrates that while the distribution of cave $\delta^{18}O_{dw}$ values shifts significantly during ENSO extremes, the amplitude of the ENSO-related cave $\delta^{18}O_{dw}$ anomalies differs up to ~6.0‰ across the system during any one time. These conclusions hold true for the subset of Mulu cave drips that feed actively accreting stalagmites (Figure S7). Other studies that capture individual ENSO events in rainfall, cave drip water, soil water, and/or stalagmite $\delta^{18}O$ time series also document responses of different amplitudes (Chen and Li, 2018; Sun et al., 2018). As such, single stalagmite $\delta^{18}O$ records from tropical (Lachniet et al., 2004; Chen et al., 2016) and subtropical (Zhao et al. 2015) regions that aim to reconstruct changes in ENSO variability through time may plausibly reflect changes in karst residence times. Our results indicate that accurate stalagmite $\delta^{18}O$-based reconstructions of past ENSO-related hydrological variations at a given site require the generation of records from multiple stalagmites at a given site, to rule out the influence of drip-site specific changes in residence time. This strategy follows on the success of well-replicated stalagmite $\delta^{18}O$ records of centennial- to millennial-scale at the Gunung Mulu (Carolin et al., 2013; 2016; Partin et al., 2007; 2013a). Unfortunately, fast-growing samples capable of resolving ENSO variability are quite rare (Orland et al., 2014), such that it might be more practical to focus on assessing common trends in ENSO-related variability between

reconstruction sites, and between proxy types, than to pursue multiple high-resolution stalagmite $\delta^{18}O$ records from the same site. In that case, proxy system forward models (Evans et al., 2013; Dee et al., 2015) of the rainwater-to-drip water $\delta^{18}O$ transformation at stalagmite $\delta^{18}O$ reconstruction sites would accelerate progress towards the identification and intercomparison of ENSO-related signals in a network of stalagmite $\delta^{18}O$ reconstructions. Likewise, such forward models are critical to the intercomparison of ENSO reconstructions derived from multiple proxy types such as corals (Tudhope et al., 2001; Cobb et al., 2003; 2013; Grothe et al., 2019; McGregor et al., 2013), lake sediments (Conroy et al., 2008), and single forams (Leduc et al., 2009; White et al., 2018).

5. Conclusions

Long-term monitoring of rainwater and drip water $\delta^{18}O$ at Gunung Mulu National Park enables the quantification of karst residence times ranging from ~3 to 18 months . Simple linear transformation of amount-weighted rainfall $\delta^{18}O$ to drip water $\delta^{18}O$ capture ~75-85% of the variance expressed at three drip sites in our study. ENSO extremes are associated with local rainfall $\delta^{18}O$ anomalies of ~6-8‰, and drip water $\delta^{18}O$ anomalies of ~3-5‰, where the magnitude of the peaks correspond to ENSO strength. One of the three long-term drip monitoring sites exhibits nonstationary behavior in karst residence times, implying time-varying contributions from a well-mixed longer-term karst water reservoir. As such, our results suggest that while stalagmite $\delta^{18}O$ records from Gunung Mulu are prime candidates for ENSO reconstruction, multiple stalagmite $\delta^{18}O$ records are required to assess the robustness of such

reconstructions. Lastly, our work demonstrates the utility of site-specific, long-term monitoring of rainfall and cave drip water $\delta^{18}O$ to inform the climatic interpretation of stalagmite $\delta^{18}O$ records.

Acknowledgements

We wish to thank Gina Moseley, Nele Meckler, Stacy Carolin, Syria Lejau, Stein-Erik Lauritzen, Robbie Shone, and Jan Berndorff for field work assistance, and all of the staff at Gunung Mulu National Park World Heritage for their dedicated assistance in keeping us safe during field expeditions. We also are extremely grateful to the Mulu Meteorological Station staff for faithfully overseeing the collection of daily rainfall samples for the last 12 years. We also acknowledge the Mulu Caves Project for their invaluable information on characterizing the Mulu karst system. We would also like to thank Hussein Sayani for his assistance in water isotope analyses. Permits for this work were granted by the Malaysian Economic Planning Unit, the Sarawak State Planning Unit, and the Sarawak Forestry Department. This work was supported by NSF grants 0645291 and 1502830 awarded to K.M.C**..** All data are publicly available on PANGAEA (https://www.pangaea.de), all rainfall data are publicly available on IAEA-WISER (https://nucleus.iaea.org/wiser/index.aspx), and all data are contained in supplementary files associated with this article. The authors acknowledge no conflicts of interest.

References

Aggarwal, P. K., Romatschke, U., Araguas-Araguas, L., Belachew, D., Longstaffe, F. J., Berg, P., Schumacher, C., and Funk, A. (2016). Proportions of convective and stratiform precipitation revealed in water isotope ratios. *Nature Geoscience*, *9*(8), 624.

Akers, P. D., Brook, G. A., Railsback, L. B., Liang, F., Iannone, G., Webster, J. W., Reeder, P.P, Cheng, H., and Edwards, R. L. (2016). An extended and higher-resolution record of climate and land use from stalagmite MC01 from Macal Chasm, Belize, revealing connections between major dry events, overall climate variability, and Maya sociopolitical changes. *Palaeogeography, palaeoclimatology, palaeoecology*, *459*, 268-288.

Baker, A., and Brunsdon, C. (2003). Non-linearities in drip water hydrology: an example from Stump Cross Caverns, Yorkshire. *Journal of Hydrology*, *277*(3-4), 151-163.

Baker, A., Hartmann, A., Duan, W., Hankin, S., Comas-Bru, L., Cuthbert, M. O., Treble, P.C., Banner, J., Genty, D., Baldini, L.M., Bartolomé, M., Moreno, A., Pérez-Mejias, C., and Werner, M. (2019). Global analysis reveals climatic controls on the oxygen isotope composition of cave drip water. *Nature communications*, *10*(1), 2984.

Beal, L. K., Wong, C. I., Bautista, K. K., Jenson, J. W., Banner, J. L., Lander, M. A., Gingerich, S.B., Partin, J.W., Hardt, B., and van Oort, N. H. (2019). Isotopic and geochemical assessment of the sensitivity of groundwater resources of Guam, Mariana Islands, to intra-and inter-annual variations in hydroclimate. *Journal of hydrology*, *568*, 174-183.

Bretherton, C.S., Widmann, M., Dymnikov, V.P, Wallace, J.M., Blade, I., (1999). Effective number of degrees of freedom of a spatial field. *J. Clim.*, 12, 1990 – 2009.

Burns, S. J., Matter, A., Frank, N., & Mangini, A. (1998). Speleothem-based paleoclimate record from northern Oman. *Geology*, *26*(6), 499-502.

Cai, B., Pumijumnong, N., Tan, M., Muangsong, C., Kong, X., Jiang, X., and Nan, S. (2010). Effects of intraseasonal variation of summer monsoon rainfall on stable isotope and growth rate of a stalagmite from northwestern Thailand. *Journal of Geophysical Research: Atmospheres*, *115*(D21).

Cai, Z., and Tian, L. (2016). Processes governing water vapor isotope composition in the Indo-Pacific region: convection and water vapor transport. *Journal of Climate*, *29*(23), 8535-8546.

Carolin, S. A., Cobb, K. M., Adkins, J. F., Clark, B., Conroy, J. L., Lejau, S., Malang, J., and Tuen, A. A. (2013). Varied response of western Pacific hydrology to climate forcings over the last glacial period. *Science*, *340*(6140), 1564-1566.

Carolin, S. A., Cobb, K. M., Lynch-Stieglitz, J., Moerman, J. W., Partin, J. W., Lejau, S., Malang, J., Clark, B., Tuens, A.A., and Adkins, J. F. (2016). Northern Borneo stalagmite records

reveal West Pacific hydroclimate across MIS 5 and 6. *Earth and Planetary Science Letters*, *439*, 182-193.

Chen, S., Hoffmann, S. S., Lund, D. C., Cobb, K. M., Emile-Geay, J., and Adkins, J. F. (2016). A high-resolution speleothem record of western equatorial Pacific rainfall: Implications for Holocene ENSO evolution. *Earth and Planetary Science Letters*, *442*, 61-71.

Chen, C. J., and Li, T. Y. (2018). Geochemical characteristics of cave drip water respond to ENSO based on a 6-year monitoring work in Yangkou Cave, Southwest China. *Journal of hydrology*, *561*, 896-907.

Cheng, H., Sinha, A., Cruz, F. W., Wang, X., Edwards, R. L., d'Horta, F. M., Ribas, C.C., Vuille, M., Stott, L.D., and Auler, A. S. (2013). Climate change patterns in Amazonia and biodiversity. *Nature communications*, *4*, 1411.

Cheng, H., Sinha, A., Wang, X.F., Cruz, F.W., Edwards, R.L. (2012). The global paleomonsoon as seen through speleothem records from Asia and the Americas. *Climate Dynamics*, 39:1045 – 62.

Cobb, K. M., Charles, C. D., Cheng, H., and Edwards, R. L. (2003). El Niño/Southern Oscillation and tropical Pacific climate during the last millennium. *Nature*, *424*(6946), 271-276.

Cobb, K. M., Adkins, J. F., Partin, J. W., and Clark, B. (2007). Regional-scale climate influences on temporal variations of rainwater and cave dripwater oxygen isotopes in northern Borneo. *Earth and Planetary Science Letters*, *263*(3-4), 207-220.

Cobb, K. M., Westphal, N., Sayani, H. R., Watson, J. T., Di Lorenzo, E., Cheng, H., Edwards, R.L., Charles, C. D. (2013). Highly variable El Niño–Southern Oscillation throughout the Holocene. *Science*, *339*(6115), 67-70.

Conroy, J. L., Overpeck, J. T., Cole, J. E., Shanahan, T. M., & Steinitz-Kannan, M. (2008). Holocene changes in eastern tropical Pacific climate inferred from a Galápagos lake sediment record. *Quaternary Science Reviews*, *27*(11-12), 1166-1180.

Craig, H. (1961). Isotopic variations in meteoric waters. *Science*, *133*(3465), 1702-1703.

Cruz Jr, F. W., Burns, S. J., Karmann, I., Sharp, W. D., Vuille, M., Cardoso, A. O., Ferrari, J.A., Silva Dias, P.L., and Viana Jr, O. (2005). Insolation-driven changes in atmospheric circulation over the past 116,000 years in subtropical Brazil. *Nature*, *434*(7029), 63.

Cuthbert, M. O., Baker, A., Jex, C. N., Graham, P. W., Treble, P. C., Andersen, M. S., and Acworth, R. I. (2014). Drip water isotopes in semi-arid karst: implications for speleothem paleoclimatology. *Earth and Planetary Science Letters*, *395*, 194-204.

Dansgaard, W. (1964). Stable isotopes in precipitation. *Tellus*, *16*(4), 436-468.

Dansgaard, W., Johnsen, S. J., Clausen, H. B., Dahl-Jensen, D., Gundestrup, N. S., Hammer, C. U., Hvldberg, C.S., Steffensen, J.P., Sveinbjörnsdottir, A.E., Jouzel, J., and Bond, G. (1993). Evidence for general instability of past climate from a 250-kyr ice-core record. *Nature*, *364*(6434), 218.

Dee, S., Emile-Geay, J., Evans, M. N., Allam, A., Steig, E. J., & Thompson, D. M. (2015). PRYSM: An open-source framework for PRoxY System Modeling, with applications to oxygen-isotope systems. *Journal of Advances in Modeling Earth Systems*, *7*(3), 1220-1247.

Griffiths, M. L., Drysdale, R. N., Gagan, M. K., Zhao, J. X., Ayliffe, L. K., Hellstrom, J. C., Hantoro, W.S., Frisia, S., Feng, Y.-x, Cartwright, I., Pierre, E. S., Fischer, M.J., and Suwargadi, B.W. (2009). Increasing Australian–Indonesian monsoon rainfall linked to early Holocene sea-level rise. *Nature Geoscience*, *2*(9), 636.

Grothe, P. R., Cobb, K. M., Liguori, G., Di Lorenzo, E., Capotondi, A., Lu, Y., Cheng, H., Edwards, L.R., Southon, J.R., Santos, G.M., Deocampo, D. M., Lynch-Stieglitz, J., Chen, T., Sayani, H., Thompson, D.M., Conroy, J.L., Moore, A.L., Townsend, K., Hagos, M., O'Conner, G., and Toth, L.T. (2019). Enhanced El Niño-Southern Oscillation variability in recent decades. *Geophysical Research Letters*, 46, doi: 10.1029/2019GL083906

Fairchild, I. J., Smith, C. L., Baker, A., Fuller, L., Spötl, C., Mattey, D., and McDermott, F. (2006). Modification and preservation of environmental signals in speleothems. *Earth-Science Reviews*, *75*(1-4), 105-153.

Fairchild, I. J., & Baker, A. (2012). *Speleothem science: from process to past environments* (Vol. 3, 1st ed.). Wiley, Oxford, UK. 432 pp.

Fleitmann, D., Burns, S. J., Neff, U., Mudelsee, M., Mangini, A., and Matter, A. (2004). Palaeoclimatic interpretation of high-resolution oxygen isotope profiles derived from annually laminated speleothems from Southern Oman. *Quaternary Science Reviews*, *23*(7-8), 935-945.

Ford, D., and Williams, P. D. (2007). *Karst hydrogeology and geomorphology* (1st ed.). Wiley, Chichester, England. 578 pp.

Frappier, A. B., Sahagian, D., Carpenter, S. J., González, L. A., and Frappier, B. R. (2007). Stalagmite stable isotope record of recent tropical cyclone events. *Geology*, *35*(2), 111-114.

Griffiths, M. L., Drysdale, R. N., Gagan, M. K., Zhao, J. X., Ayliffe, L. K., Hellstrom, J. C., Hantoro, W.S., Frisia, S., Feng, Y.-x, Cartwright, I., Pierre, E. S., Fischer, M.J., and Suwargadi, B.W. (2009). Increasing Australian–Indonesian monsoon rainfall linked to early Holocene sea-level rise. *Nature Geoscience*, *2*(9), 636.

Grothe, P. R., Cobb, K. M., Liguori, G., Di Lorenzo, E., Capotondi, A., Lu, Y., Cheng, H., Edwards, L.R., Southon, J.R., Santos, G.M., Deocampo, D. M., Lynch-Stieglitz, J., Chen, T., Sayani, H., Thompson, D.M., Conroy, J.L., Moore, A.L., Townsend, K., Hagos, M., O'Conner, G., and Toth, L.T. (2019). Enhanced El Niño-Southern Oscillation variability in recent decades. *Geophysical Research Letters*, 46, doi: 10.1029/2019GL083906

Heinrich, H. (1988). Origin and consequences of cyclic ice rafting in the northeast Atlantic Ocean during the past 130,000 years. *Quaternary research*, *29*(2), 142-152.

Jones, I. C., Banner, J. L., and Humphrey, J. D. (2000). Estimating recharge in a tropical karst aquifer. *Water Resources Research*, *36*(5), 1289-1299.

Kennett, D. J., Breitenbach, S. F., Aquino, V. V., Asmerom, Y., Awe, J., Baldini, J. U., Bartlein, P., Culleton, B.J., Ebert, C., Jazwa, C., Macri, M. J., Marwan, N., Polyak, V., Prufer, K.M., Ridley, H.E., Sodemann, H., Winterhalder, B., and Huag, G.H. (2012). Development and disintegration of Maya political systems in response to climate change. *Science*, *338*(6108), 788-791.

Konecky, B. L., Noone, D. C., and Cobb, K. M. (2019). The Influence of Competing Hydroclimate Processes on Stable Isotope Ratios in Tropical Rainfall. *Geophysical Research Letters*, *46*(3), 1622-1633.

Kurita, N., Horikawa, M., Kanamori, H., Fujinami, H., Kumagai, T. O., Kume, T., and Yasunari, T. (2018). Interpretation of El Niño–Southern Oscillation-related precipitation anomalies in north-western Borneo using isotopic tracers. *Hydrological Processes*, *32*(14), 2176-2186.

Lachniet, M. S., Bernal, J. P., Asmerom, Y., Polyak, V., and Piperno, D. (2012). A 2400 yr Mesoamerican rainfall reconstruction links climate and cultural change. *Geology*, *40*(3), 259-262.

Lachniet, M.S. (2009). Climatic and environmental controls on speleothem oxygen-isotope values. *Quaternary Science Reviews*, *28*(5-6), 412 – 432.

Lachniet, M. S., Burns, S. J., Piperno, D. R., Asmerom, Y., Polyak, V. J., Moy, C. M., and Christenson, K. (2004). A 1500-year El Niño/Southern Oscillation and rainfall history for the isthmus of Panama from speleothem calcite. *Journal of Geophysical Research: Atmospheres*, *109*(D20).

Lases-Hernandez, F., Medina-Elizalde, M., Burns, S., and DeCesare, M. (2019). Long-term monitoring of drip water and groundwater stable isotopic variability in the Yucatán Peninsula: Implications for recharge and speleothem rainfall reconstruction. *Geochimica et Cosmochimica Acta*, *246*, 41-59.

Leduc, G., Vidal, L., Cartapanis, O., & Bard, E. (2009). Modes of eastern equatorial Pacific thermocline variability: Implications for ENSO dynamics over the last glacial period. *Paleoceanography*, *24*(3).

Liu, S., Peng, X., Chen, Q., Qin, S., Zhao, J., Feng, Y., Luo, S., and Zhou, H. (2018). The 1997–1998 El Niño event recorded by a stalagmite from central China. *Quaternary international*, *487*, 71-77.

McDonald, J., Drysdale, R., Hill, D., Chisari, R., and Wong, H. (2007). The hydrochemical response of cave drip waters to sub-annual and inter-annual climate variability, Wombeyan Caves, SE Australia. *Chemical Geology*, *244*(3-4), 605-623.

Meckler, A. N., Clarkson, M. O., Cobb, K. M., Sodemann, H., and Adkins, J. F. (2012). Interglacial hydroclimate in the tropical West Pacific through the Late Pleistocene. *Science*, *336*(6086), 1301-1304.

Medina-Elizalde, M., Burns, S. J., Lea, D. W., Asmerom, Y., von Gunten, L., Polyak, V., Vuille, M., and Karmalkar, A. (2010). High resolution stalagmite climate record from the Yucatán Peninsula spanning the Maya terminal classic period. *Earth and Planetary Science Letters*, *298*(1-2), 255-262.

Mickler, P. J., Banner, J. L., Stern, L., Asmerom, Y., Edwards, R. L., and Ito, E. (2004). Stable isotope variations in modern tropical speleothems: evaluating equilibrium vs. kinetic isotope effects. *Geochimica et Cosmochimica Acta*, *68*(21), 4381-4393.

Moerman, J. W., Cobb, K. M., Adkins, J. F., Sodemann, H., Clark, B., and Tuen, A. A. (2013). Diurnal to interannual rainfall δ18O variations in northern Borneo driven by regional hydrology. *Earth and Planetary Science Letters*, *369*, 108-119.

Moerman, J. W., Cobb, K. M., Partin, J. W., Meckler, A. N., Carolin, S. A., Adkins, J. F., Lejau, S., Malang, J., Clark, B., and Tuen, A. A. (2014). Transformation of ENSO-related rainwater to dripwater δ18O variability by vadose water mixing. *Geophysical Research Letters*, *41*(22), 7907-7915.

Muangsong, C., Cai, B., Pumijumnong, N., Hu, C., and Cheng, H. (2014). An annually laminated stalagmite record of the changes in Thailand monsoon rainfall over the past 387 years and its relationship to IOD and ENSO. *Quaternary international*, *349*, 90-97.

McGregor, H. V., Fischer, M. J., Gagan, M. K., Fink, D., Phipps, S. J., Wong, H., & Woodroffe, C. D. (2013). A weak El Niño/Southern Oscillation with delayed seasonal growth around 4,300 years ago. *Nature Geoscience*, *6*(11), 949-953.

Nott, J., Haig, J., Neil, H., and Gillieson, D. (2007). Greater frequency variability of landfalling tropical cyclones at centennial compared to seasonal and decadal scales. *Earth and Planetary Science Letters*, *255*(3-4), 367-372.

Orland, I.J., Burstyn, Y., Bar-Matthews, M., Kozdon, R., Ayalon, A., Matthews, A., Valley, J.W. (2014). Seasonal climate signals (1990 – 2008) in a modern Soreq Cave stalagmite as revealed by high-resolution geochemical Analysis. Chem. Geol. 363, 203 – 215.

Partin, J. W., Cobb, K. M., Adkins, J. F., Clark, B., and Fernandez, D. P. (2007). Millennial-scale trends in west Pacific warm pool hydrology since the Last Glacial Maximum. *Nature*, *449*(7161), 452.

Partin, J. W., Jenson, J. W., Banner, J. L., Quinn, T. M., Taylor, F. W., Sinclair, D., Hardt, B., Lander M.A., Bell, T., Miklavic, B., Jocson, J. M., and Taborosi, D. (2012). Relationship between modern rainfall variability, cave dripwater, and stalagmite geochemistry in Guam, USA. *Geochemistry, Geophysics, Geosystems*, *13*(3).

Partin, J. W., Cobb, K. M., Adkins, J. F., Tuen, A. A., and Clark, B. (2013a). Trace metal and carbon isotopic variations in cave dripwater and stalagmite geochemistry from northern Borneo. *Geochemistry, Geophysics, Geosystems*, *14*(9), 3567-3585.

Partin, J. W., Quinn, T. M., Shen, C. C., Emile-Geay, J., Taylor, F. W., Maupin, C. R., Lin, K., Jackson, C.S., Banner, J.L., Sinclair, D.J., Huh, C. A. (2013b). Multidecadal rainfall variability in South Pacific Convergence Zone as revealed by stalagmite geochemistry. *Geology*, *41*(11), 1143-1146.

Rozanski, K., Araguas-Araguas, L., and Gonfiantini, R. (1992). Relation between long-term trends of oxygen-18 isotope composition of precipitation and climate. *Science*, *258*(5084), 981-985.

Sinha, A., Cannariato, K. G., Stott, L. D., Li, H. C., You, C. F., Cheng, H., Edwards, R.L., Singh, I. B. (2005). Variability of Southwest Indian summer monsoon precipitation during the Bølling-Allerød. *Geology*, *33*(10), 813-816.

Sun, Z., Yang, Y., Zhao, J., Tian, N., and Feng, X. (2018). Potential ENSO effects on the oxygen isotope composition of modern speleothems: Observations from Jiguan Cave, central China. *Journal of hydrology*, *566*, 164-174.

Treble, P. C., Bradley, C., Wood, A., Baker, A., Jex, C. N., Fairchild, I. J., Gagan, M.K., Cowley, J., and Azcurra, C. (2013). An isotopic and modelling study of flow paths and storage in Quaternary calcarenite, SW Australia: implications for speleothem paleoclimate records. *Quaternary Science Reviews*, *64*, 90-103.

Tudhope, A. W., Chilcott, C. P., McCulloch, M. T., Cook, E. R., Chappell, J., Ellam, R. M., Lea, D.W., Lough, J.M, and Shimmield, G. B. (2001). Variability in the El Niño-Southern Oscillation through a glacial-interglacial cycle. *Science*, *291*(5508), 1511-1517.

Wang, X., Auler, A. S., Edwards, R. L., Cheng, H., Ito, E., and Solheid, M. (2006). Interhemispheric anti-phasing of rainfall during the last glacial period. *Quaternary Science Reviews*, *25*(23-24), 3391-3403.

Wang, Y. J., Cheng, H., Edwards, R. L., An, Z. S., Wu, J. Y., Shen, C. C., and Dorale, J. A. (2001). A high-resolution absolute-dated late Pleistocene monsoon record from Hulu Cave, China. *science*, *294*(5550), 2345-2348.

White, S. M., Ravelo, A. C., & Polissar, P. J. (2018). Dampened El Niño in the early and mid-Holocene due to insolation-forced warming/deepening of the thermocline. *Geophysical Research Letters*, *45*(1), 316-326.

Zhang, J., and Li, T.Y. (2019). Seasonal and interannual variations of hydrochemical characteristics and stable isotopic compositions of drip waters in Furong Cave, Southwest China based on 12 years' monitoring. *Journal of Hydrology*. 572. 10.1016/j.jhydrol.2019.02.052.

Zhao, K., Wang, Y., Edwards, R. L., Cheng, H., Liu, D., & Kong, X. (2015). A high-resolved record of the Asian Summer Monsoon from Dongge Cave, China for the past 1200 years. *Quaternary Science Reviews*, *122*, 250-257.

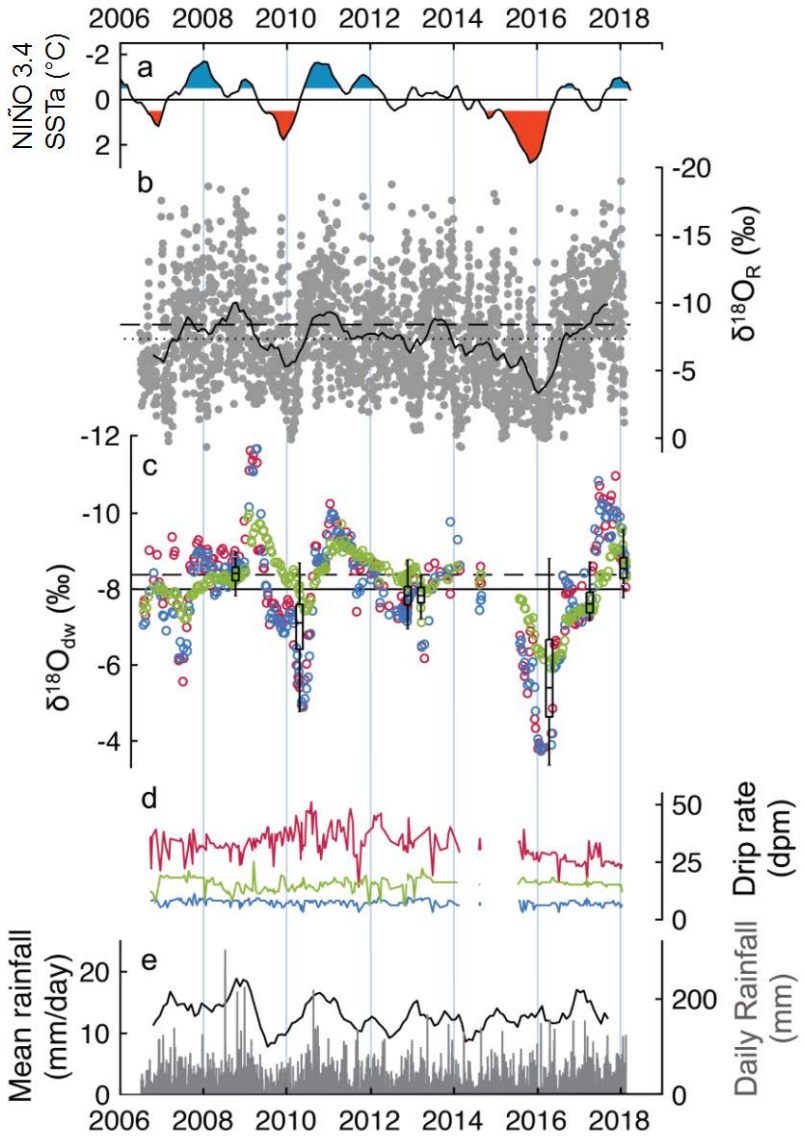

Figure 1 | N. Gunung Mulu rainfall and cave drip water oxygen isotope time series. (a) NIÑO 3.4 SSTa index (ERSSTv5, Huang et al., 2017), plotted as a 3-month running average. Red (blue) coloring indicates warm (cold) ENSO anomalies based on a threshold of +0.5ºC (–0.5 ºC). (b) Mulu daily rainfall $\delta^{18}O$ (grey circles, non-amount-weighted) plotted with a 7-month running mean (black line). Non-amount weighted average $\delta^{18}O_R$ for the entire time series is indicated by a dotted line (-7.3 ± 3.7‰) while the amount-weighted average $\delta^{18}O_R$ is indicated

by a dashed line (–8.4 ± 2.4‰). (c) Mulu cave $\delta^{18}O_{dw}$ from Wind Fast (WF; maroon circles), Wind Slow (WS; blue circles), and Lang's Cave (L2; green circles). The solid line indicates the $\delta^{18}O_{dw}$ averaged across all three drips (–8.0 ± 1.2‰), while the dashed line represents the amount-weighted $\delta^{18}O_R$ average plotted in (b). Box (25^{th}-75^{th} quartiles) and whiskers (total range, excluding outliers, see Figure S5) represent $\delta^{18}O_{dw}$ values from 7 spatial drip surveys. (d) Drip rate in drips per minute (dpm) for the three time series drips plotted in (c), plotted in the corresponding color. (e) Daily Mulu rainfall amount (grey bars) plotted with the 7 month running average (solid black line). Y-axes in panels A, B, and C are inverted. Monthly ERSSTv5 data found online at https://www.cpc.ncep.noaa.gov/data/indices/ersst5.nino.mth.81-10.ascii.

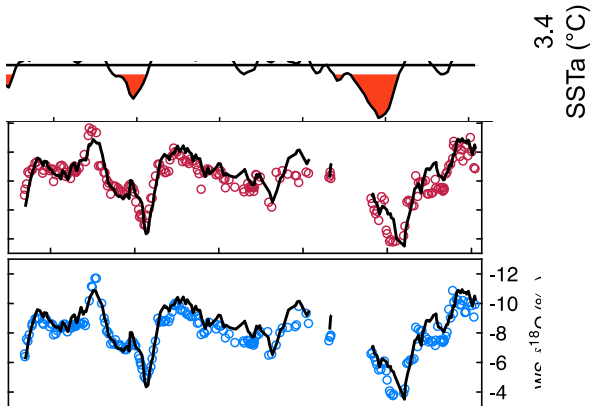

Figure 2 | Observed versus modelled Mulu drip water $\delta^{18}O$ time series. (a) The top panel is NIÑO3.4 SSTa index (ERSSTv5, Huang et al., 2017), plotted as a 3-month running average with a one month overlap. Red (blue) coloring indicates warm (cold) ENSO anomalies based on a threshold of +0.5ºC (–0.5 ºC). (b) Observed (open circles) and modelled (black line) $\delta^{18}O_{dw}$ for

drips Wind Fast (WF; maroon) and (c) Wind Slow (WS; blue), where both panels b and c are plotted with a residence time of 4.5 months from the autogenic recharge model. (d) Observed (open circles) $\delta^{18}O_{dw}$ for Lang's Cave (L2; green) with modelled $\delta^{18}O_{dw}$ (black line) using a residence time of 10.5 months from the autogenic recharge model. (e) Observed (open circles) $\delta^{18}O_{dw}$ for Lang's Cave (L2; green) with modelled $\delta^{18}O_{dw}$ from the bivariate mixing model (dual-reservoir). For pink and purple (maroon) lines, residence time selected is 10.5 months (16.75 months). Reservoir A=10.5 or 16.75 months from the autogenic recharge model and Reservoir B is the Mulu amount-weighted rainfall $\delta^{18}O$ mean (-8.4‰). An A:B mixing ratio of 40:60 (purple line) and an A:B mixing ratio of 80:20 (pink and maroon lines) provide an optimal data fit. Note that y-axes are inverted in all panels and different y-axes scalings.